Substituent Effect on the Luminescent Properties of a Series of Deep Blue Emitting Mixed Ligand Ir(III) Complexes

Yi-Yeol Lyu,[†,‡] Younghun Byun,[†] Ohyun Kwon,[†] Eunsil Han,[†] Woo Sung Jeon,[†] Rupasree Ragini Das,*[,†] and Kookheon Char*[,‡]

Samsung Advanced Institute of Technology, P.O. Box 111, Suwon 440-600, Korea, and School of Chemical and Biological Engineering and NANO System Institute-National Core Research Center, Seoul National University, Seoul 151-744, Korea

Received: December 22, 2005

The syntheses of the bright deep blue emitting mixed ligand Ir(III) complexes comprising two cyclometalating, one phosphine and one cyano, ligands are reported. In this study, a firm connection between the nature of the excited states and the physicochemical behavior of the complexes with different ligand systems is elucidated by correlating the observed crystal structures, spectroscopic properties, and electrochemical properties with the theoretical results obtained by the density functional theory (DFT) methods. The cyclometalating ligands used here are the anions of 2-(4′,6′-difluorophenyl)-pyridine (F_2ppy), 2-(4′,6′-difluorophenyl)-4-methyl pyridine (F_2ppyM), and 4-amino-2-(4′,6′-difluorophenyl)-pyridine ($DMAF_2$ppy). The phosphine ligands are PhP(O−$(CH_2CH_2O)_3$−$CH_3)_2$ and $Ph_2P(O-(CH_2CH_2O)_n-CH_3)$, where Ph = phenyl and n = 1 (**P1**), 3 (**P3**), or 8 (**P350**). The thermal stabilities of the complexes were enhanced upon increasing the "n" value. The crystal structures of the complexes, [($DMAF_2$ppy)$_2$Ir(P1)CN], **(P1)DMA**, and [(F_2ppyM)$_2$Ir(P3)CN], **(P3)F2M**, show the cyano and phosphine groups being in a cis configuration to each other and in a trans configuration to the coordinating C_{ring} atoms. The long Ir−C_{ring} bond lengths are ascribed to the *trans effect* of the strong phosphine and cyano ligands. DFT calculations indicate that the highest occupied molecular orbital (HOMO) is mainly contributed from the d-orbitals of the iridium atom and the π-orbitals of cyclometalating and cyano ligands, whereas the lowest unoccupied molecular orbital (LUMO) spreads over only one of the cyclometalating ligands, with no contribution from phosphine ligands to both frontier orbitals. Dimethylamino substitution increases the energy of the emitting state that has more metal-to-ligand-charge-transfer (MLCT) character evidenced by the smaller vibronic progressions, smaller difference in the ^{1}MLCT and ^{3}MLCT absorption wavelengths, and higher extinction coefficients (ϵ) than the F_2ppy and F_2ppyM complexes. However, the increase in the basicity of the dimethylamino group in the $DMAF_2$ppy complexes in the excited states leads to distortions and consequent nonradiative depopulation of the excited states, decreasing their lower photoluminescence (PL) efficiency. The effect of the substituents in the phosphine ligand is more pronounced in the electroluminescence (EL) than in the PL properties. Multilayer organic light emitting devices (OLEDs) are fabricated by doping the Ir(III) complexes in a blend of *m*CP (*m*-bis(*N*-carbazolyl benzene)) and polystyrene, and their device characteristics are studied. The **(P3)F2M** complex shows a maximum external quantum efficiency (η_{ex}) of 2%, a maximum luminance efficiency (η_L) of 4.13 cd/A at 0.04 mA/cm^2, and a maximum brightness of 7200 cd/m^2 with a shift of the Commission Internationale de L'Eclairage (CIE) coordinates from (0.14, 0.15) in film PL to (0.19, 0.34) in EL.

Introduction

The photophysics and electroluminescence of cyclometalated heavy transition metal complexes have drawn much attention since the utilization of the green emitting phosphorescent, tris-cyclometalated Ir(III) complex, $Ir(ppy)_3$,[1] as a dopant in organic light emitting devices (OLEDs).[2] Due to the strong spin−orbit coupling constant of these heavy transition metals, the singlet and triplet metal-to-ligand-charge-transfer (MLCT) states are mixed together, and the triplet MLCT state (^{3}MLCT) can emit effectively by burrowing the intensity from the singlet MLCT state (^{1}MLCT).[3] These complexes are able to provide 100% internal efficiency, as they can utilize both the singlet and triplet excitons on the host material through the Förster and Dexter energy transfer.[4] For the development of full color phosphorescent light emitting devices, the realization of all three green,[5] red,[6] and blue[7] (RGB) colors is necessary.

The colors of phosphorescent complexes used in such devices are tuned by the variation of both cyclometalating and ancillary ligands.[8,9] Until now, several small molecular and polymeric blue emitting phosphorescent complexes[7,10,11] have been reported, but the realization of highly efficient deep blue emission is still a challenge to achieve. Both phosphine and cyano groups are known as very strong field ligands, and their inclusion in the coordination sphere can increase the highest occupied molecular orbital (HOMO)−lowest unoccupied molecular orbital (LUMO) gap to achieve the hypsochromic shift in the emission color.[12] Ir(III) complexes of *N*-phenyl pyrazole and

* To whom correspondence should be addressed. E-mail: rd.rupasree@samsung.com (R.R.D.); khchar@plaza.snu.ac.kr (K.C.).
† Samsung Advanced Institute of Technology.
‡ Seoul National University.

10.1021/jp057446s CCC: $33.50
Published on Web 05/10/2006

CHART 1

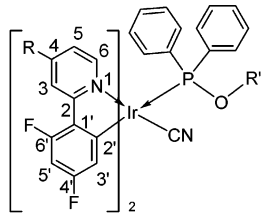

R = H, R' = -$(CH_2CH_2O)_3$-CH_3 ; **(P3)F2**
R = CH_3, R' = -$(CH_2CH_2O)_3$-CH_3 ; **(P3)F2M**
R = NMe_2, R' = -(CH_2CH_2O)-CH_3 ; **(P1)DMA**
R = NMe_2, R' = -$(CH_2CH_2O)_3$-CH_3 ; **(P3)DMA**
R = NMe_2, R' =-$(CH_2CH_2O)_n$-CH_3 (average Mn = 350); **(P350)DMA**

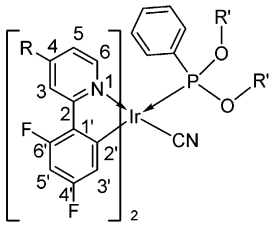

R = H,
R' = -$(CH_2CH_2O)_3$-CH_3 ; **(P3)2F2**

its derivatives are reported to emit in the deep blue and ultraviolet region.[14,15] There are also instances of the osmium compounds consisting of the strong field carbonyl ligand emitting in the deep blue region.[13] However, the simultaneous improvement of the Commission Internationale de L'Eclairage (CIE) coordinates and efficiencies of the blue emitting phosphorescent metal complexes for their use in OLEDs is still a critical issue. As good photoluminescence (PL) efficiency, short PL lifetime, significant metal-to-ligand-chrge-transfer (MLCT) contribution to the emitting state, and electrochemical stability of the cyclometalated Ir(III) complexes are key factors for the choice of a triplet emitter in the phosphorescent organic light emitting devices, it is very essential to assess these properties for different cyclometalating and ancillary ligand systems. In the previous reports of the excited state properties of Ir(III) complexes,[11] Ir(III) is bis-cyclometalated and complexed to a chelating ancillary ligand or two similar monodentate ancillary ligands. So far, there is no detailed report of the structure−photophysical relationship of the complexes consisting of three different types of ligands. To this end, we attempted to synthesize a series of new deep blue emitting bis-cyclometalated Ir(III) complexes consisting of strong field ligands such as triphenylphosphine and cyano groups (Chart 1).

To achieve deep blue emission, we substituted the 4-position of the pyridyl ring of the 2-(4′,6′-difluorophenyl)-pyridine (F_2ppy) ligand by electron-donating groups such as methyl and dimethyl amino groups. One or two of the phenyl groups in triphenyl phosphine were replaced by $O-(CH_2CH_2O)_n-CH_3$ ($n = 1$, 3, or 8) groups. We tried to correlate the observed crystal structures and spectroscopic properties with the theoretical results obtained by the density functional theory (DFT) methods. Nonetheless, the dimethyl amino-substituted complexes shifted the peak emission by 10 nm more than the methyl-substituted complex but suffered from more nonradiative emission contrary to the "energy gap law". The DFT studies suggested that an increase in the electron density on the dimethyl amino group in the excited state leading to distortions is the cause of higher nonradiative radiations of the dimethyl amino-substituted complexes. The complexes emit strongly both in the solution and solid state from an admixture of ^{3}MLCT and ligand $\pi-\pi^*$ state in the blue region with the CIE coordinates from (0.15, 0.09) to (0.14, 0.16), with the peak emissions being in the range 434−472 nm. We fabricated polymer phosphorescent light emitting devices[16−18] using the Ir(III) complexes as dopants and a blend of polystyrene and the *m*CP (*m*-bis(*N*-carbazolyl benzene))[19] as the host materials. Here, polystyrene acts as a binding polymer for the dopant and the host *m*CP. We did not use poly(9-vinylcarbazole) (PVK) as the host or binder, since its triplet energy[20] is less than those of the complexes in the present study, with there being a possibility of a decrease in the device efficiency by backward energy transfer[21] from the dopants. Efficient energy transfer from *m*CP to all of the dopants was observed in the electroluminescence (EL) spectra. We observed an increasing order of the PL and EL efficiency in the sequence **(P3)F2M** > **(P3)F2** > **(P3)DMA** (Chart 1), showing better efficiency in the case of the methyl-substituted complex. To check the effect of the substituents on the phosphine ligand, we varied the $-(CH_2CH_2O)-$ units in the glycolic substituents on phosphines of the dimethylamino-substituted complexes and observed that an increase in the number of $-(CH_2CH_2O)-$ units gave better device efficiency. However, higher efficiency was marked for the **(P3)F2** based device as compared with that of the **(P3)2F2** complex probably due to there being less charge conduction in the latter instance.

Synthesis

The starting materials $[Ir(F_2ppy)_2Cl]_2$, $[Ir(MeF_2ppy)_2Cl]_2$, and $[Ir(DMAF_2ppy)_2Cl]_2$ (F_2ppy, F_2ppyM, and $DMAF_2$ppy are the anions of 4′,6′-difluoro-2-phenylpyridine, 4′,6′-difluoro-4-methyl-2-phenylpyridine, and 4′,6′-difluoro-4-diaminomethyl-2-phenylpyridine, respectively) were synthesized from $IrCl_3 \cdot 3H_2O$ (Acros Chemicals), and the cyclometalating ligands 4′,6′-difluoro-2-phenylpyridine, 4′,6′-difluoro-4-methyl-2-phenylpyridine, and 4′,6′-difluoro-4-diaminomethyl-2-phenylpyridine were synthesized on the basis of the literature procedure.[22] The syntheses of the phosphine ligands **P1**, **P3**, and **P350** and synthetic scheme of the complexes are given in the Supporting Information.

[Ir(DMAF$_2$ppy)$_2$(P3)CN], (P3)DMA. To a solution of ligand **P3** (0.907 mmol, 0.316 g) in 200 mL of tetrahydrofuran was added the dimer $[Ir(DMAF_2ppy)_2Cl]_2$ (0.411 mmol, 0.57 g). The mixture was stirred at ambient temperature for 18 h under a nitrogen environment. Evaporation of the solvent afforded a yellow solid. The crude product was chromatographed on silica with 5−10% methanol in dichloromethane as the eluent to the $[Ir(DMAF_2ppy)_2$**(P3)**Cl] complex as a yellow solid (0.59 g, 69%). The $[Ir(DMAF_2ppy)_2$**(P3)**Cl] complex (0.500 mmol, 0.52 g) was dissolved in 50 mL of tetrahydrofuran, and then, potassium cyanide (5.00 mmol, 0.34 g) in 50 mL of methanol was added thereto and stirred at ambient temperature for 16 h under a nitrogen environment. To the reaction mixture, *n*-hexane was added when the desired product was precipitated as a yellow solid. It was chromatographed on silica with 5−10% methanol in dichloromethane as the eluent to give the complex, [Ir(DMAF$_2$-ppy)$_2$**(P3)**CN], as a light yellow solid (0.29 g, 56%). ^{1}H NMR (300 MHz, CH_2Cl_2): δ (ppm) 8.74 (d, 1H), 8.50 (d, 1H), 7.88 (d, 2H), 7.59 (m, 1H), 7.45 (m, 3H), 7.22 (t, 1H), 7.07 (t, 2H), 7.01 (m, 1H), 6.92 (t, 2H), 6.33 (m, 3H), 6.08 (d, 1H), 5.91 (d, 1H), 5.67 (t, 1H), 3.70 (m, 1H), 3.48 (11H, m), 3.46 (s, 3H), 3.16 (s, 6H), 3.04 (s, 6H). ^{31}P NMR (300 MHz, CH_2Cl_2): δ (ppm) 88.27. Coordination induced shift (CIS) = −25.78. ES

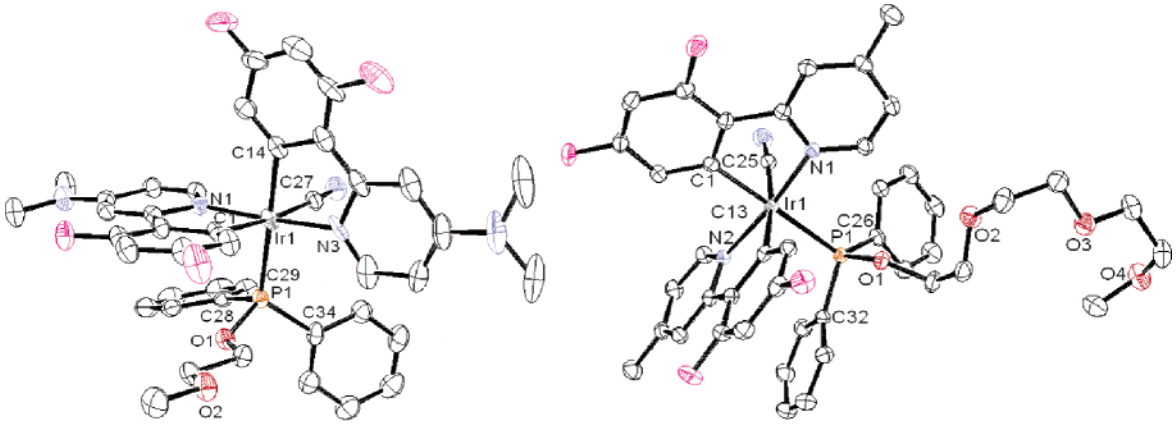

Figure 1. ORTEP diagrams of the complexes **(P1)DMA** and **(P3)F2M** with 50% probability with atom labeling. Hydrogen atoms are omitted for clarity.

mass spectroscopy: calculated molecular weight (M_w) = 1033.081, *m/e* = 1034.499 $[M + H]^+$. Dissociation temperature (T_d), 257 °C. Anal. Calcd: C (%), 53.48; H (%), 4.59; N (%), 6.78. Found: C (%), 53.28; H (%), 4.60; N (%), 6.70.

[Ir(DMAF$_2$ppy)$_2$(P1)CN], (P1)DMA. The [Ir(DMAF$_2$ppy)$_2$-**(P1)**CN] complex was synthesized in the same manner as [Ir(DMAF$_2$ppy)$_2$**(P3)**CN], except that **P1** was used instead of **P3**. Light yellow solid (0.27 g, 57%). ^{1}H NMR (300 MHz, CH_2Cl_2): δ (ppm) 8.76 (d, 1H), 8.50 (d, 1H), 7.88 (d, 2H), 7.59 (m, 1H), 7.45 (m, 3H), 7.22 (t, 1H), 7.07 (t, 2H), 7.01 (m, 1H), 6.92 (t, 2H), 6.33 (m, 3H), 6.08 (d, 1H), 5.91 (d, 1H), 5.67 (t, 1H), 3.70 (m, 1H), 3.52 (11H, m), 3.30 (s, 3H), 3.28 (s, 2H), 3.16 (s, 6H), 3.04 (s, 6H). ^{31}P NMR (300 MHz, CH_2Cl_2): δ (ppm) 88.43. CIS = −25.57. ES mass spectroscopy: calculated M_w = 944.976, *m/e* = 946.479 $[M + H]^+$. T_d, 286 °C. Anal. Calcd: C (%), 53.38; H (%), 4.16; N (%), 7.41. Found: C (%), 53.29; H (%), 4.15; N (%), 7.34.

[Ir(DMAF$_2$ppy)$_2$(P350)CN], (P350)DMA. The [Ir(DMAF$_2$-ppy)$_2$**(P350)**CN] complex was synthesized in the same manner as [Ir(DMAF$_2$ppy)$_2$**(P3)**CN], except that **P350** was used instead of **P3**. Light yellow solid (0.26 g, 43%). ^{1}H NMR (300 MHz, CH_2Cl_2): δ (ppm) 8.73 (d, 1H), 8.50 (d, 1H), 7.86 (t, 1H), 7.58 (m, 1H), 7.41 (m, 3H), 7.22 (t, 1H), 7.07 (t, 2H), 7.01 (m, 1H), 6.92 (t, 2H), 6.33 (m, 3H), 6.08 (d, 1H), 5.91 (d, 1H), 5.67 (t, 1H), 3.70 (m, 1H), 3.50 (27H, m), 3.33 (s, 3H), 3.16 (s, 6H), 3.04 (s, 6H). ^{31}P NMR (300 MHz, CH_2Cl_2): δ (ppm) 89.67. CIS = −24.29. T_d, 298 °C.

[Ir(F$_2$ppy)$_2$(P3)CN], (P3)F2. The [Ir(F$_2$ppy)$_2$**(P3)**CN] complex was synthesized in the same manner as the [Ir(DMAF$_2$-ppy)$_2$**(P3)**CN] complex, except that [Ir(F$_2$ppy)$_2$Cl]$_2$ was used instead of [Ir(DMAF$_2$ppy)$_2$Cl]$_2$. Yellow solid (0.30 g, 63%). ^{1}H NMR (300 MHz, CH_2Cl_2): δ (ppm) 9.40 (d, 1H), 9.20 (d, 1H), 8.38 (d, 1H), 7.89 (m, 3H), 7.58 (d, 1H), 7.54 (m, 2H), 7.47 (m, 2H), 7.24 (m, 2H), 7.05 (t, 2H), 6.91 (t, 1H), 6.81 (t, 2H), 6.78 (m, 2H), 5.82 (d, 1H), 5.40 (t, 1H), 3.60 (1H, m), 3.50 (s, 11H), 3.32 (s, 3H). ^{31}P NMR (300 MHz, CH_2Cl_2): δ (ppm) 87.70. CIS = −26.29. ES mass spectroscopy: calculated M_w = 946.945, *m/e* = 948.451 $[M + H]^+$. T_d, 247 °C. Anal. Calcd: C (%), 53.27; H (%), 3.94; N (%), 4.44. Found: C (%), 53.32; H (%), 3.98; N (%), 4.41.

[Ir(F$_2$ppy)$_2$(P3)2CN], (P3)2F2. The complex [Ir(F$_2$ppy)$_2$-**(P3)2**CN] was synthesized in the same manner as the complex [Ir(F$_2$ppy)$_2$**(P3)**CN], except that **(P3)2** was used instead of **P3**. Yellow solid (0.31 g, 60%). ^{1}H NMR (300 MHz, CH_2Cl_2): δ (ppm) 9.68 (d, 1H), 9.27 (d, 1H), 8.34 (d, 1H), 7.87 (m, 2H), 7.62 (t, 1H), 7.34 (t, 1H), 7.20 (t, 1H), 7.03 (m, 3H), 6.78 (t, 2H), 6.41 (m, 2H), 5.77 (d, 1H), 5.41 (t, 1H), 4.75 (m, 1H), 4.27 (m, 1H), 4.18 (m, 1H), 3.79 (m, 3H), 3.62 (m, 14H), 3.49 (m, 4H), 3.30 (s, 3H). ^{31}P NMR (300 MHz, CH_2Cl_2): δ (ppm) 113.61. CIS = +90.05. ES mass spectroscopy: calculated M_w = 1033.033, *m/e* = 1034.499 $[M + H]^+$. T_d, 293 °C. Anal. Calcd: C (%), 49.99; H (%), 4.59; N (%), 4.07. Found: C (%), 49.97; H (%), 4.59; N (%), 4.04.

[Ir(F$_2$ppyM)$_2$(P3)CN], (P3)F2M. The complex [Ir(MeF$_2$-ppy)$_2$**(P3)**CN] was synthesized in the same manner as the complex [Ir(DMAF$_2$ppy)$_2$**(P3)**CN], except that [Ir(MeF$_2$-ppy)$_2$Cl]$_2$ was used instead of [Ir(DMAF$_2$ppy)$_2$Cl]$_2$. Light yellow solid (0.28 g, 57%). ^{1}H NMR (300 MHz, CH_2Cl_2): δ (ppm) 9.18 (d, 1H), 8.96 (d, 1H), 8.21 (1H, s), 7.88 (t, 2H), 7.59 (s, 1H), 7.52 (d, 1H), 7.47 (m, 2H), 7.24 (t, 1 H), 7.05 (t, 2H), 6.98 (d, 1H), 6.81 (t, 2H), 6.73 (d, 1H), 6.43 (m, 2H), 5.83 (d, 1H), 3.59 (m, 1H), 3.49 (m, 11H), 3.32 (s, 6H), 2.58 (s, 3H), 2.41 (s, 3H). ^{31}P NMR (300 MHz, CH_2Cl_2): δ (ppm) 87.78. CIS = −26.21. ES mass spectroscopy: calculated M_w = 974.999, *m/e* = 976.435 $[M + H]^+$. T_d, 250 °C. Anal. Calcd: C (%), 54.20; H (%), 4.24; N (%), 4.31. Found: C (%), 54.20; H (%), 4.25; N (%), 4.27.

Results and Discussion

Crystal Structure. The ORTEP diagrams of the complexes are presented in Figure 1. Crystallographic data and selected geometrical parameters are given in Tables 1 and 2, respectively. In both cases, the Ir(III) center is octahedrally coordinated to one phosphine, one cyano group, and two cyclometalating ligands. The molecules possess distorted octahedral geometry due to the coordination of nonequivalent cyano and bulky phosphine ligands. The **(P1)DMA** complex crystallizes in the monoclinic system with four molecules per unit cell. On the other hand, **(P3)F2M** forms a triclinic crystal with two molecules per unit cell. The complexes exhibit a trans-P,C configuration, retaining the cis-C,C and trans-N,N configuration of the chlorobridged dimer. The Ir−C bonds (Ir−C_{av} = 2.048 Å for **(P3)F2M**, Ir−C_{av} = 2.056 Å for **(P1)DMA**) are close to the reported values of 2.02−2.13 Å for the dimeric complexes[25] and the mononuclear complexes containing the Ir(ppy)$_2$ fragments[26,27] but longer than the bis-cyclometalated acac complexes.[11] The Ir−N bonds of these complexes (Ir−N_{av} = 2.064 Å for **(P3)F2M**, Ir−N_{av} = 2.061 Å for **(P1)DMA**) are longer than the Ir−C bonds, similar to the observations in the dimeric complexes and monomeric complexes.[26,27] Following are the discussions on the important features observed from the crystal structure of the complexes:

(1) The Ir−CN bond is longer than the trans Ir−C (ring) bond in both **(P3)F2M** and **(P1)DMA**. It indicates the greater

TABLE 1: Crystal Data and Summary of Structure Refinements for P(1)DMA and P(3)F2M

	P(1)DMA	P(3)F2M
empirical formula	C43 H43 F4 Ir N5 O3 P	C44 H41 F4 Ir N3 O5 P
formula weight	976.99	990.97
temperature	173(2) K	173(2) K
wavelength	0.71073 Å	0.71073 Å
crystal system	monoclinic	triclinic
space group	$P2_1/n$	Pi
unit cell dimensions	$a = 13.410(2)$ Å, $\alpha = 90°$ $b = 14.547(2)$ Å, $\beta = 103.798(3)°$ $c = 21.170(4)$ Å, $\gamma = 90°$	$a = 9.7070(8)$ Å, $\alpha = 86.8940(10)°$ $b = 10.2082(8)$ Å, $\beta = 88.988(2)°$ $c = 19.8603(16)$ Å, $\gamma = 88.887(2)°$
volume	4010.6(12) Å^3	1964.4(3) Å^3
Z	4	2
density (calculated)	1.618 Mg/m^3	1.675 Mg/m^3
absorption coefficient	3.434 mm^{-1}	3.509 mm^{-1}
$F(000)$	1952	988
crystal size	0.68 × 0.50 × 0.10 mm^3	0.55 × 0.33 × 0.33 mm^3
theta range for data collection	1.64−28.30°	2.00−28.31°
index ranges	$-16<=h<=17$, $-16<=k<=19$, $-28<=l<=27$	$-12<=h<=11$, $-13<=k<=13$, $-25<=l<=26$
reflections collected	22546	12424
independent reflections	9397 [R(int) = 0.0355]	8936 [R(int) = 0.0113]
completeness to theta = 28.30°	94.2%	91.5%
absorption correction	semiempirical from equivalents	semiempirical from equivalents
max and min transmission	0.7252 and 0.2036	0.3905 and 0.2484
refinement method	full-matrix least squares on F^2	full-matrix least squares on F^2
data/restraints/parameters	9397/0/602	8936/0/526
goodness of fit on F^2	1.219	1.064
final R indices [$I > 2$sigma(I)]	R1 = 0.0567, wR2 = 0.1247	R1 = 0.0193, wR2 = 0.0481
R indices (all data)	R1 = 0.0623, wR2 = 0.1271	R1 = 0.0203, wR2 = 0.0485
largest diff. peak and hole	3.993 and −2.549 e·Å^{-3}	1.556 and −0.823 e·Å^{-3}

TABLE 2: Experimental and Calculated Values of Selected Bond Lengths (Å) and Angles (deg) of the (P1)DMA and (P3)F2M Complexes

bond distance			bond angle		
	calcd	exptl		calcd	exptl
			(P1)DMA		
Ir−C_1	2.075	2.058	C_1−Ir−C_{14}	87.9	87.2
Ir−N_1	2.087	2.059	C_{14}−Ir−C_{27}	89.0	88.6
Ir−C_{14}	2.052	2.054	C_1−Ir−C_{27}	172.9	173.1
Ir−N_3	2.105	2.073	C_1−Ir−P	94.5	92.8
Ir−C_{27}	2.071	2.066	C_{14}−Ir−P	177.5	179.4
Ir−P	2.455	2.346	C_{27}−Ir−P	88.6	91.3
			O_1−P_1−C_{28}	97.4	97.5
			O_1−P_1−C_{34}	101.5	102.8
			O_1−P_1−Ir	117.7	117.9
			C_{28}−P−C_{34}	100.7	99.3
			(P3)F2M		
Ir−C_1	2.052	2.052	C1−Ir−C13	90.2	88.2
Ir−N_1	2.103	2.076	C1−Ir−C25	87.0	86.7
Ir−C_{13}	2.070	2.045	C13−Ir−C25	172.8	172.4
Ir−N_2	2.083	2.052	C1−Ir−P	177.5	174.9
Ir−C_{25}	2.071	2.059	C13−Ir−P	89.3	87.2
Ir−P	2.443	2.356	C25−Ir−P	93.7	98.1
			O1−P−C26	104.2	104.9
			O1−P−C32	102.8	104.1
			O1−P−Ir	107.4	107.8
			C26−P−C32	103.5	103.9

σ-donation of the aromatic ring carbon as compared with that of the CN ligand.

(2) All of the Ir−C bonds are shorter than the Ir−P bonds due to the smaller radius of carbon than phosphorus.

(3) Slight variations in Ir−CN and Ir−P bond lengths in **(P3)F2M** and **(P1)DMA** are observed. This could be due to the combined effect of the substituents on the cyclometalating as well as phosphine ligands.

(4) The S−P−S bond angles (S = substituent on phosphorus) are different for the two complexes. As observed from the crystal structure, two of the S−P−S bond angles in **P(1)DMA**, for instance, the O(1)−P(1)−C(28) and C(28)−P(1)−C(34) angles, are 97.5(2) and 99.3(3)°, respectively, whereas all of the S−P−S bond angles in **(P3)F2M** are around 104°. On the basis of the bond angles, it can be inferred that the **P3** ligand imposes a steric crowding in **(P3)F2M** compared with the **P1** ligand in **(P1)DMA**. The σ-forward bonding and the π-back-bonding of the Ir−P bond could be affected due to the larger size of the **P3** ligand, resulting in a weaker Ir−P bond. This effect is reflected in the Ir−P bond lengths in both complexes, which are 2.536(4) Å for **(P3)F2M** and 2.346(1) Å for **(P1)DMA**, accounting for the stronger Ir−P bond in **(P1)DMA**. ^{31}P NMR shows a large positive coordination induced shift (CIS) of +90.05 for **(P3)2F2**, whereas the other four complexes show negative coordination shifts in the range −24.3 to −26.3 ppm. A positive CIS indicates the structural constraints of the molecule requiring the contraction of the S−P−S bond angle in the complex.[28] However, the negative CIS values are attributed to the S−P−S angle opening after complexation.

(5) We observe a free outward extension of the −O−CH2−CH2−OCH3 group away from the P atom, with the two O atoms being trans to each other in the **(P1)DMA**. However, for the case of **(P3)F2M**, the ethylene glycol groups form a half crown ether-like structure.

(6) The distortion away from the CCCP square plane is less for **(P1)DMA** and more for **(P3)F2M**. The planes containing Ir and ring carbons and Ir, cyano carbons, and phosphorus subtend at an angle of 4.7° for the **(P1)DMA** complex. The corresponding angle for **(P3)F2M** is 5.2°. Similarly, the subtend angles for the planes containing Ir, ring carbons, and cyano carbons and Ir, ring carbons, and phosphorus are 5.3 and 9.2° for the **(P1)DMA** and **(P3)F2M** complexes, respectively. The extent of bowing of the axial square plane of CCCP in the complexes is due to crystal packing forces and possibly dependent on both cyclometalating and phosphine ligands.

DFT Calculations. The ground state geometries of the Ir(III) complexes were fully optimized without any symmetry constraints at the DFT level[29,30] by using the B3LYP functional.[31]

Four Ir(III) complexes, **(P1)DMA**, **(P3)DMA**, **(P1)F2M**, and **(P3)F2M**, were considered to compare the influences of dimethylamino (DMA) and methyl (Me) substituents as well as the ethylene glycol group on the electronic properties of Ir(III) complexes. A relativistic effective core potential (ECP) on the Ir atom[32] replaced the inner core electrons, and double-ζ quality basis sets (LANL2DZ) were employed for the outer core $[(5s)^2(5p)^6]$ electrons and the $(5d)^6$ valence electrons, while the 6-31G(d) basis set was applied for the ligand atoms. At the respective optimized geometries of the singlet ground state, time-dependent DFT (TDDFT) calculations[33,34] using the B3LYP functional with the same basis set were carried out in order to obtain the vertical excitation energies of singlet (S_n) and triplet (T_n) states. Calculated S_n and T_n energies are compared with the experimental ones. All calculations were performed by the Gaussian 98 program.[35]

The calculated and experimental geometrical parameters of the complexes **(P1)DMA** and **(P3)F2M** are summarized in Table 2. The overall geometrical parameters of the calculated structures of the complexes **(P1)DMA** and **(P3)F2M** are in quite good agreement with those of the crystal structures. For instance, the calculated Ir−C bond distances for **(P1)DMA** are 2.075 and 2.052 Å, which are quite comparable with the corresponding experimental values, 2.058 and 2.054 Å, respectively. The calculated bond angles are also well matched with the experimental data. In comparison of DMA- and Me-substituted complexes, the Ir−N distances of Me-substituted complexes (**(P1)F2M** and **(P3)F2M**) are slightly longer than those of DMA-substituted complexes (**(P1)DMA** and **(P3)DMA**), similar to the experimental observation. The steric hindrance of the longer ethylene glycolic group may slightly distort the octahedral environment of the Ir complex; the deviation of the square planarity of CCCP is calculated to be 6.5° for **(P3)DMA** which is larger than that of **(P1)DMA** (4.2°). The deviations of the square planarity for **(P1)F2M** and **(P3)F2M** are also calculated to be 3.8 and 8.6°, respectively, and are in qualitative agreement with the corresponding experimental values of 5.2 and 4.7° for **(P3)F2M** and **(P1)DMA**, respectively.

The highest occupied molecular orbitals (HOMOs) and the lowest unoccupied molecular orbitals (LUMOs) of **(P1)DMA**, **(P3)DMA**, **(P1)F2M**, and **(P3)F2M** are shown in Figure 2. Both the HOMOs and LUMOs demonstrate π-symmetry. The HOMO represents a mixture of the phenyl ring of the cyclometalating ligand and cyano orbitals, while the LUMO is predominantly a cyclometalating ligand in character.[36] There are reports of varied distributions of HOMOs and LUMOs[9,11,32] on cyclometalating as well as ancillary ligands. It is interesting to know that in the bis-cyclometalated tertiary butyl isocyanide complexes[11] the tertiary butyl isocyanide ligand does not contribute to the HOMO or the LUMO, but in the present case, the cyano group participates in the HOMO, consequent upon which it could influence the MLCT character of the complexes. It is noted that the LUMO is concentrated on only a single cyclometalating ligand and LUMO+1 is localized on the other cyclometalating ligand. It has been reported that the LUMO in the bis-cyclometalated complexes consisting of two similar cyclometalated ligands and two similar ancillary ligands[11] or symmetric acac ligands[32] reside on both of the cyclometalated ligands. In this present investigation, the two cyclometalating ligands are similar but the ancillary ligands (phosphine and cyano) are different, which may result in the contribution of each cyclometalating ligand being separated into LUMO and LUMO+1 (the energy difference between LUMO and LUMO+1 is calculated to be 0.09 eV).

The calculated triplet energy of 2.92 eV (424 nm) for **(P3)F2M** is comparable to the experimental triplet energy of 2.79 eV (444 nm) and the onset of absorption band at 390 nm (3.18 eV). The calculated triplet energy of **(P1)DMA** (3.08 eV, 401 nm) is comparable to the experimental value of 2.88 eV (430 nm) and is very close to the onset of the absorption maximum at 390 nm (3.18 eV). The calculated singlet absorption of **(P3)F2M** at 318 nm has a significant oscillator strength (f = 0.05) and is close to the experimental singlet absorption at 308 nm (extinction coefficient, $\epsilon = 6000\ \text{mol}^{-1}\ \text{cm}^{-1}$). On the other hand, the singlet absorptions at 362, 353, and 335 nm obtained from the TDDFT calculations have very small oscillator strengths of 0.025, 0.017, and 0.001, respectively, and correspond to the experimental absorption features in the region 325−375 nm. As the absorptions in this region have very low extinction coefficients (ϵ = 500−1900 $\text{mol}^{-1}\ \text{cm}^{-1}$), the transitions are suggested to have more triplet character and less singlet character. Thus, in the shorter wavelength region, the absorption bands can be of more singlet MLCT character than those in the longer wavelength region. Similar assessments and assignments can be applied to the calculated singlet absorptions of **(P1)DMA** at 334 (f = 0.061), 328 (f = 0.005), 321 (f = 0.08), and 314 nm (f = 0.09) and experimental absorptions in the regions 325−370 and 290−310 nm, respectively. **(P3)F2M** is assigned with a maximum triplet energy of 3.409 eV (368 nm) by TDDFT calculations. We presume that this corresponds to the ^{3}MLCT absorption peak at 345 nm, as demonstrated in the solution absorption spectra (Figure 4A). However, **(P1)DMA** does not show clearly resolved ^{3}MLCT absorption peaks; instead, a broad band is observed in the region 321−374 nm with a shoulder around 345 nm. The Gaussian decomposition of this broad absorption band showed two peaks at 324 and 347 nm (inset of Figure 5a). The peak at 324 nm is close to the ^{1}MLCT absorption peak, whereas the peak at 347 nm with almost half of the intensity of the 324 nm peak can be ascribed to the ^{3}MLCT absorption. This absorption wavelength is very close to ^{3}MLCT absorption at 364 nm suggested by TDDFT calculations.

Electrochemical Properties. The redox potentials of these complexes are summarized in Table 3. The electrochemical oxidation processes were monitored by cyclovoltammetry. The cyclic voltammetric patterns of the **(P3)F2**, **(P3)2F2**, and **(P3)F2M** complexes are similar to one another, where re-reduction waves of the oxidized species are not observed even at a scan rate (υ) of 10 V s^{-1} (Figure 3A−C). This is presumably due to the weaker metal−ligand interaction involving phosphines as reported in the irreversible oxidation processes in cyclometalated Pt(II) phosphine complexes.[38] The cyclic voltammetric patterns of **(P1)DMA**, **(P3)DMA**, and **(P350)DMA** complexes are also similar to one another, but the enhancement of the reversibility of oxidation waves for the +1/0 redox couple is clearly observed at a υ value of 10 V s^{-1} (Figure 3D−F). Judging from the i_{pc}/i_{pa} ratio depending on υ, the half-lifes (τ) of the cation radicals of the **(P1)DMA**, **(P3)DMA**, and **(P350)DMA** complexes are in the range between 0.01 and 0.1 s.[39] Such kinetic stabilization phenomena of the radical cations can also be ascribed to the stronger electron-donating ability of the $DMAF_2ppy$ ligand as compared with that of the F_2ppy or MeF_2ppy ligand.

The anodic peak potential (E_{pa}) values for the **(P1)DMA**, **(P3)DMA**, **(P350)DMA**, **(P3)F2**, **(P3)2F2**, and **(P3)F2M** complexes are 0.93, 0.94, 0.95, 1.17, 1.21, and 1.14 V versus Fc/Fc^+, respectively. The **(P3)F2**, **(P3)2F2**, and **(P3)F2M** complexes show higher oxidation potentials compared with the

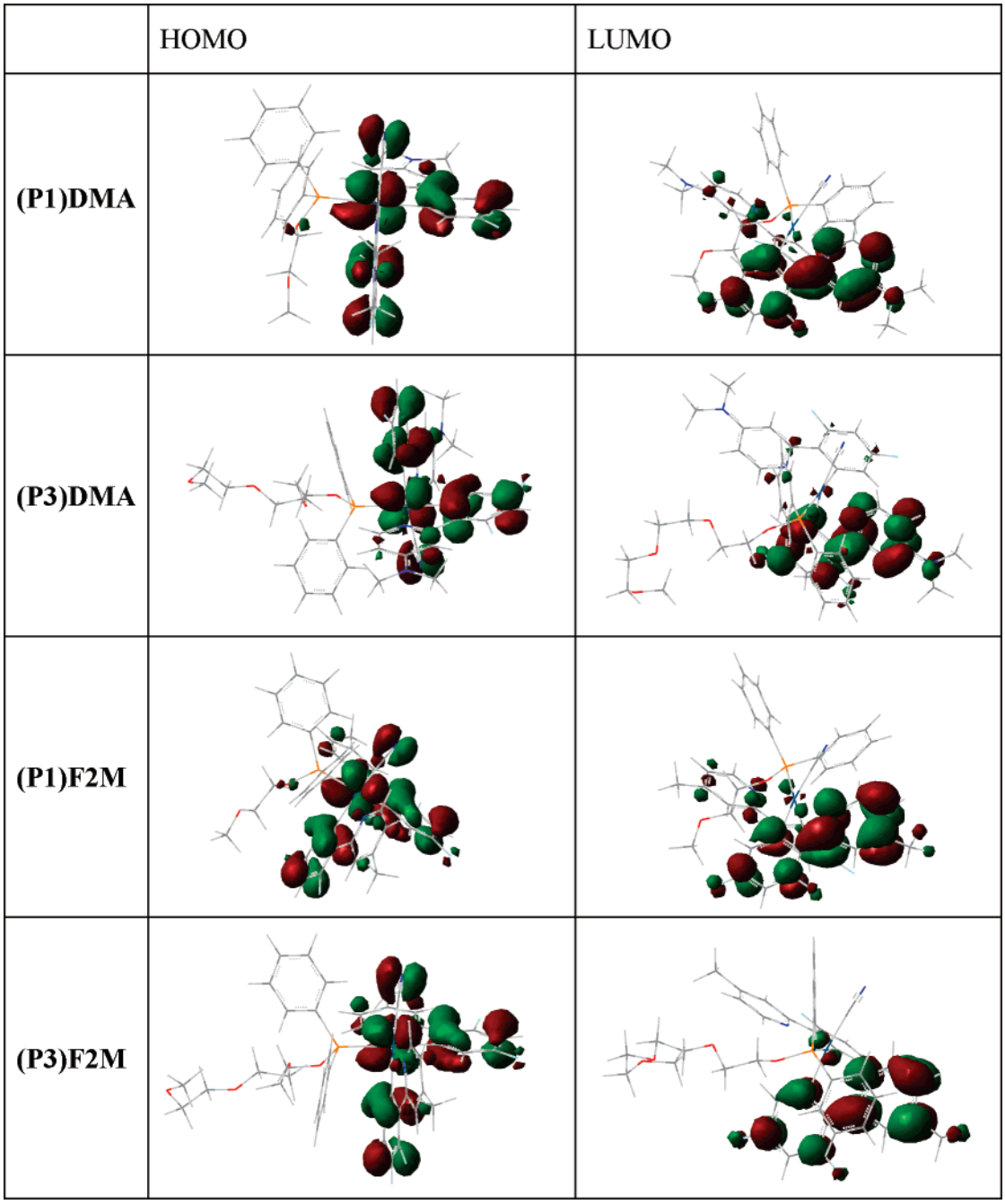

Figure 2. Calculated frontier orbitals of **(P1)DMA**, **(P3)DMA**, **(P1)F2M**, and **(P3)F2M**.

(P1)DMA, **(P3)DMA**, and **(P350)DMA** complexes mainly due to the stronger electron-donating ability of the $DMAF_2ppy$ ligand than that of the F_2ppy or MeF_2ppy ligand. Comparison of **(P3)-DMA**, **(P3)F2M**, and **(P3)F2** indicates that the coordination of $DMAF_2ppy$ and MeF_2ppy ligands shifts the oxidation potential by 0.24 and 0.03 V, respectively, toward the negative direction, facilitating easier oxidation, compared with the coordination of the F_2ppy ligand. This is also substantiated by the DFT calculations that the Ir(III) center and pyridyl nitrogen have charge densities of +0.260 and −2.016, respectively, in the **(P3)DMA** complex, whereas those in the **(P3)F2M** complex have charge densities of +0.267 and −1.669, respectively. The **(P1)DMA**, **(P3)DMA**, and **(P350)DMA** complexes show nearly the same oxidation potentials, implying that the number of $-(CH_2CH_2O)-$ units has little effect on the HOMO level of the complexes. It is also supported by the similar absorption and emission features of the **(P1)DMA**, **(P3)DMA**, and **(P350)-DMA** complexes containing the $DMAF_2ppy$ ligand. In this study, the HOMO is assigned to an admixture of the d-orbital of metal and π-orbitals of the cyclometalating and CN ligands as found from the DFT calcualtions, which goes parallel with the shift of oxidation potentials depending on the electronic effects of the substituents on the pyridyl ring.

The electrochemical reduction properties of these complexes were examined by cyclovoltammetry and Osteryoung square wave voltammetry (OSWV). Even though all of the complexes exhibited redox potentials near the limit of the potential window of tetrahydrofuran (THF), it was hard to obtain well-defined cyclic voltammograms due to the unstable base current originated from the solvent decomposition. In Osteryoung square wave voltammetry (OSWV), suppression of the base current can be achieved, as the base current decays more rapidly than the Faradaic current, after the application of a voltage pulse to the electrode. Thus, measurements of the current a short time

TABLE 3: Energy Levels and Photophysical and Electrochemical Data of the Complexes

compound	λ_{abs}[a] (nm)	λ_{em}[b] (nm) CIE[h] (x, y)	λ_{em}[c] (nm) CIE[h] (x, y)	ΦPL[d] (%, ±5)	Stoke's shift (cm^{-1})	τ[d] (μs)	K_r (10^4 s^{-1})	K_{nr} (10^5 s^{-1})	$E_{1/2}$[e] (oxd) (V)	$E_{1/2}$[f] (red) (V)	HOMO[g] (eV)	LUMO[h] (eV)	triplet energy (eV)
P(1)DMA	229, 272, 331, 347	434, 452 (0.15, 0.09)	434, 452 (0.15, 0.09)	30	5944	3.89	7.7	1.8	0.93	−2.91	6.23	3.43	2.8
P(3)DMA	228, 271, 332, 347	434, 452 (0.15, 0.09)	434, 452 (0.15, 0.09)	30	5944	4.63	6.4	1.5	0.94	−2.91	6.24	3.44	2.8
P(350)DMA	228, 271, 332, 347	434, 452 (0.15, 0.09)	434, 452 (0.15, 0.09)	24	5944	3.64	6.5	2.0	0.95	−2.92	6.25	3.45	2.8
P(3)F2	241, 261, 307, 350	445, 472 (0.14, 0.16)	449, 472 (0.14, 0.16)	62	6100	10.44	5.9	0.36	1.17	−2.52 −2.86	6.47	3.69	2.78
P(3)2F2	240, 257, 308, 347	444, 471 (0.14, 0.15)	447, 470 (0.14, 0.16)	66	6395	13.82	4.7	0.24	1.21	−2.54 −2.92	6.51	3.72	2.79
P(3)F2M	242, 260, 304, 345	444, 471 (0.14, 0.15)	447, 471 (0.14, 0.16)	74	6463	8.67	8.5	0.29	1.14	−2.61 −2.96	6.44	3.65	2.79

[a,b] The spectra are monitored in 10^{-5} M solution of the complexes in CH_2Cl_2. [c] Emission peaks and CIE coordinates of the 6% doped PMMA films. [d] In PMMA films doped with 6% of the complexes. [e] Measured by the cyclovoltammetric method in acetonitrile solution using ferrocene/ferrocinium as the internal reference electrode at a scan rate of 0.1 V/s. [f] Measured by the square wave voltammetry (SWV) method in anhydrous THF solution using ferrocene/ferrocinium as the internal reference electrode at a scan rate of 0.025 V/s. The parameters of SWV are the following: step E = 25 mV, SW amplitude = ±10 mV. [g] HOMO energies are referenced to the vacuum level.[15] [h] LUMO energies are referenced to the energy of the emitting state and obtained from HOMO and emission energy.

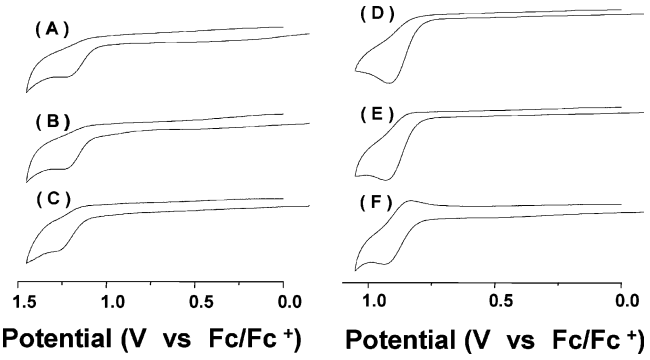

Figure 3. Effect of scan rate (υ) on cyclic voltammograms of **(P3)F2** with υ = 0.1 (A), 1 (B), and 10 (C) V s^{-1} and of **(P1)DMA** with υ = 0.1 (D), 1 (E), and 10 (F) V s^{-1}.

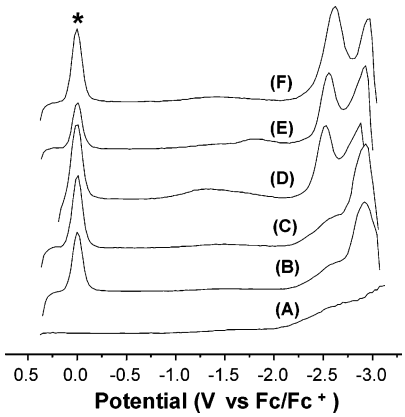

Figure 4. Osteryoung square wave voltammograms of the complexes in the reduction region: (A) blank; (B) **(P1)DMA**; (C) **(P3)DMA**; (D) **(P3)F2**; (E) **(P3)2F2**; (F) **(P3)F2M**. The ferrocenium/ferrocene reduction peak is marked with an asterisk.

before each new pulse lead to the elimination of the base current from the recorded voltammograms.[40] Typical OSW voltammograms of the complexes are shown in Figure 4. It is worth noting that the reduction processes were significantly affected by the substituted groups on the cyclometalating ligands. Two reduction processes, with potentials ranging from −2.5 to −3.0 V (vs Fc/Fc^+), were detected for the complexes **(P3)F2**, **(P3)2F2**, and **(P3)2F2M**, but only single reduction processes were observed for the **DMA** complexes. The two reduction processes in the **(P3)F2**, **(P3)2F2**, and **(P3)2F2M** complexes take place at the two cyclometalated ligands, consistent with the related cyclometalated Ir(III) complexes.[1c,3c,41] However, in the **DMA** complexes, the electron-donating dimethyl amino group on the pyridyl ring increases the electron density in the pyridyl ring and hence shifts the reduction potentials toward the negative direction. The second reduction peak could not be obtained in the limits of the potential window of the experimental conditions.

Though both methyl and dimethyl amino groups show an electron-donating effect, the dimethyl amino substitution has a more dominating effect on the redox potentials than the methyl group and results in the cathodic shifts of both of the redox potentials. Since the oxidation and reduction potentials are related to the HOMO and LUMO levels, it is evident that both the HOMO and the LUMO are raised in energy in the **DMA** complexes. The DFT calculations of these complexes indicate that the LUMO spreads over only one cyclometalating ligand. Hence, it is difficult to predict exactly whether the pyridyl or phenyl ring of the cyclometalating ligand is reduced. As the reduction potentials demonstrate a wider range (−2.5 to −2.91 V) compared with the oxidation potentials (0.91−1.21 V), it can be concluded that the LUMOs of these complexes are more affected by the substituents on the cyclometalating ligands.

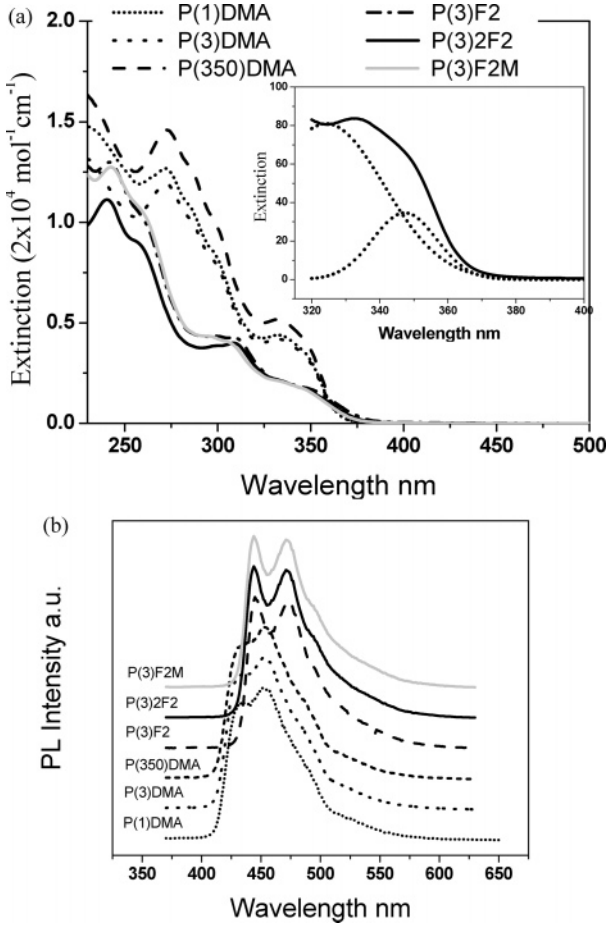

Figure 5. (a) Absorption spectra and (b) emission spectra of the complexes in 10^{-5} M solution in dichloromethane.

Photophysical Properties. The absorption and emission spectra of the complexes are summarized in Table 3 and shown in Figure 5. The absorption spectra do not extend onto the visible region and end around 390 nm in all cases. The absorption bands below 300 nm correspond to the $\pi-\pi^*$ transitions of aromatic ligands,[42] as evidenced by their high extinction coefficients. These are perturbed due to the coordination to the metal center. The bands at higher wavelengths are attributed to the metal-to-ligand-charge-transfer (MLCT) bands.[3a,d] In DMA complexes, the MLCT bands are not well resolved into ^{1}MLCT and ^{3}MLCT bands and broad bands in the region of 320−372 nm are observed, indicating the merge of ^{1}MLCT and ^{3}MLCT bands.[8a] The Gaussian decomposition of this broad absorption band showed two peaks at 324 and 347 nm (inset of Figure 5a). The peak at 324 nm is close to the ^{1}MLCT absorption, whereas the peak at 347 nm with almost half of the intensity of the 324 nm peak can be ascribed to the ^{3}MLCT absorption. This absorption wavelength is very close to ^{3}MLCT absorption at 364 nm suggested by TDDFT calculations. However, these absorption features are distinct in the **(P3)F2**, **(P3)2F2**, and **(P3)F2M** complexes. The absorption peaks corresponding to 305 (ϵ = 7600−8000 mol^{-1} cm^{-1}) and 345 (ϵ = 3200−3600 mol^{-1} cm^{-1}) nm are attributed to the ^{1}MLCT and ^{3}MLCT transition processes, respectively, as evidenced by their relative extinction coefficients.[43] In all of these complexes, we presume the participation of the cyano ligand in the charge transfer process along with Ir(III) d-orbitals and the phenyl group of the cyclometalating ligand.

All of these complexes are highly emissive both in solution and in solid state at room temperature. **(P3)F2**, **(P3)2F2**, and **(P3)F2M** exhibit two emission peaks around 444 and 471 nm with vibronic progressions of 1291 cm^{-1} and CIE coordinates of (0.14, 0.15) in dichloromethane solutions. The dichloromethane solutions of the DMA complexes, **(P1)DMA**, **(P3)DMA**, and **(P350)DMA**, also show two emission peaks around 434 and 452 nm (vibronic progression = 818 cm^{-1}) with CIE coordinates of (0.15, 0.09). As the emission energy and HOMO of the **DMA** complexes are higher than the **(P3)F2**, **(P3)2F2**, and **(P3)F2M** complexes, it is a clear observation that dimethylamino substitution raises both the HOMO and LUMO of the **(P1)DMA**, **(P3)DMA**, and **(P350)DMA** complexes (Table 3). All six complexes demonstrate shoulders around 490 nm, characteristics of the cyclometalated complexes of phenylpyridine and its derivatives. The origin of the two emission peaks was investigated by monitoring the excitation spectra at the two different peak emissions. The excitation spectra corresponding to the two peak emissions are found to be the same, confirming them as the vibronic progressions of the relaxation of the same emitting state to the different vibrational levels of the ground state.[8b] The 6% doped PMMA films of the **(P3)F2**, **(P3)2F2**, **(P3)F2M**, **(P1)DMA**, **(P3)DMA**, and **(P350)DMA** complexes exhibited almost similar emission peaks and CIE color coordinates (Table 3).

The photoluminescence (PL) quantum efficiency measurement (Table 3) of PMMA films doped with Ir(III) complexes shows that the dimethylamino (**DMA**)-substituted complexes show less than half of the quantum efficiency of **(P3)F2**, **(P3)2F2**, and **(P3)F2M**. When the $-(CH_2CH_2O)-$ repeat units were increased from $-(CH_2CH_2O)-CH_3$ in **(P1)DMA** to $-(CH_2CH_2O)_3-CH_3$ in **(P3)DMA**, the quantum efficiency did not change, but upon further increase of the $-(CH_2CH_2O)-$ units as in **(P350)DMA**, the efficiency decreased. It is interesting to see that the methyl substitution in the cyclometalating ring enhances the quantum efficiency: **(P3)F2** exhibits a quantum efficiency of 62%, whereas **(P3)F2M** shows 72%, which is the maximum value among all six complexes examined. Comparing **(P3)F2** with **(P3)2F2**, we find that the substitution of the second phenyl group in (**P3**) by the $-O-(CH_2CH_2O)_3-CH_3$ group makes the molecule **(P3)2F2** (66% quantum efficiency) more efficient than **(P3)F2** (62% quantum efficiency) in PL.

The PL lifetimes (τ) of the complexes **(P1)DMA**, **(P3)DMA**, **(P350)DMA**, **(P3)F2**, **(P3)2F2**, and **(P3)F2M** are 3.89, 4.63, 3.64, 10.44, 13.82, and 8.67 ms. From the relations

$$\Phi_{PL} = k_r/(k_r + k_{nr}) \quad \text{and} \quad \tau = 1/(k_r + k_{nr}) \qquad (1)$$

where k_r and k_{nr} are radiative and nonradiative rate constants, the k_r and k_{nr} values for these complexes are calculated (Table 3). Due to the strong spin−orbit coupling in the heavy metal complexes such as the Ru(II) and Ir(III) complexes, ^{1}MLCT and ^{3}MLCT are very much mixed so that the relaxation of energy from the ^{1}MLCT to ^{3}MLCT state in these complexes occurs in the femtosecond time scale.[44] It has been found that the Franck−Condon state accessed from photoexcitation to the emitting state evolves completely within 300 fs. The intersystem crossing from the singlet MLCT triplet MLCT is considered to be 100%.[45] Hence, the rate of intersystem crossing is not considered in the calculations of the radiative and nonradiative rate constants.

The plots of k_r and Φ_{PL} of the complexes are shown in Figure 6a. The radiative rate constants of the blue emitting cyclometalated Ir(III) complexes[9a,c] are usually of the order of 10^5 s^{-1}. The less k_r values of the complexes can be correlated with an increase of the Ir−C(ring) bond length due to the trans effect of the strong cyano and phosphine ligands. The elongation of

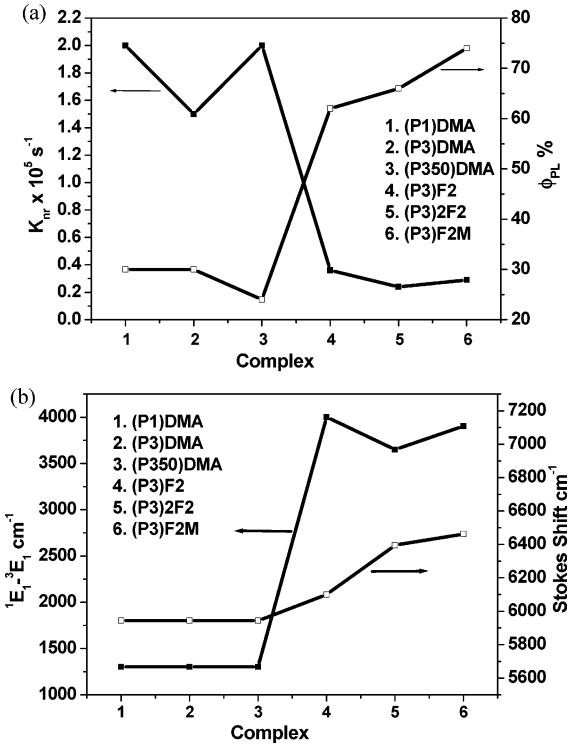

Figure 6. Comparative plot of (a) k_{nr} and PL efficiencies and (b) ($^1E_1$) − ($^3E_1$) and Stokes shifts of the complexes.

the Ir−C(ring) bond affects the metal−ligand stretching vibration and influences the vibronic coupling between the excited and ground states. We can presume that the cyano and phosphine ligands decrease the coupling between the ground and excited states, resulting in the decreased k_r values.[11] k_r increases in the sequence **(P3)F2M** (8.5×10^4 s^{-1}) > **(P3)DMA** (6.4×10^4 s^{-1}) > **(P3)F2** (5.9×10^4 s^{-1}). In the **DMA** series, the k_r values decrease in the series **(P350)DMA** ≈ **(P3)DMA** < **(P1)DMA**, indicating that the radiative emission rate decreases as the $-(CH_2CH_2O)-$ units in phosphine increase. On the same basis, the k_r value of **(P3)F2** is higher than that of the **(P3)2F2** complex. The k_{nr} values of the **(P1)DMA**, **(P3)DMA**, and **(P350)DMA** complexes are about 1 order of magnitude higher than the **(P3)F2**, **(P3)2F2**, and **(P3)F2M** complexes. This is in contrast to the energy gap law followed by a vast number of diimine transition metal complexes[46] which states that ln(k_{nr}) decreases with the increasing emission energy of the complexes. The ln(k_{nr}) values of the **(P1)DMA**, **(P3)DMA**, **(P350)DMA**, **(P3)F2**, **(P3)2F2**, and **(P3)F2M** complexes are 12.10, 11.91, 12.20, 10.49, 10.08, and 10.27, respectively. The low quantum efficiency, high k_{nr} of the **DMA** complexes could be understood from the results obtained from the DFT calculation of the **(P1)DMA** and **(P3)DMA** complexes. The HOMOs of these complexes have no contribution from the dimethylamino group of the cyclometalating ligand, whereas the LUMOs of these complexes have contribution from the dimethylamino group. This could possibly increase the basicity of the nitrogen atom of the dimethylamino group upon excitation, leading to $sp^2 \rightarrow sp^3$ rehybridization and subsequent out-of-plane distortion.[47] The distortional vibrations cause a great deal of nonradiative depopulation of the excited state, thereby decreasing the quantum efficiency. Thus, although the incorporation of a dimethyl amino group blue shifts the peak emission, it decreases the photoluminescence efficiency of the system.

All of these complexes demonstrate large Stokes shifts of 5944−6463 cm^{-1}. Stokes shift is the difference in the longest wavelength absorption energy and highest energy emission peak and is related to the degree of overlap between the molecular orbitals of the electron accepting state and the orbitals of the emitting state and hence is indicative of the singlet triplet splitting. As the singlet−triplet splitting increases, the charge transfer characteristics decrease. These large Stokes shifts indicate that these complexes emit from an admixture of MLCT and ligand $\pi-\pi^*$ state, as the Stokes shift higher than 4000 cm^{-1} is indicative of a substantial ligand $\pi-\pi^*$ contribution to the MLCT state.[8a] For the phosphorescent Ir(III) complexes, the emission lifetime correlates inversely with the singlet−triplet splitting. In the present series, we do not observe any uniform relationship of the lifetime and Stokes shift. However, the **(P3)F2**, **(P3)2F2**, and **(P3)F2M** complexes demonstrate an inverse relationship of the lifetimes and Stokes shifts.

For the phosphorescent complexes, the difference in the energies of the ^{1}MLCT ($^1E_1$) and 3MLCT ($^3E_1$) absorptions is a measure of the MLCT contribution to the emitting state. The smaller the ($^1E_1$) − ($^3E_1$) value, the greater the MLCT contribution. The **(P1)DMA**, **(P3)DMA**, and **(P350)DMA** complexes have similar ($^1E_1$) − ($^3E_1$) values (Figure 6b) of 1302 cm^{-1}, whereas for the **(P3)F2**, **(P3)2F2**, and **(P3)F2M** complexes the differences are 4002, 3649, and 3909 cm^{-1}, respectively. Thus, the ($^1E_1$) − ($^3E_1$) values of the **(P3)F2**, **(P3)2F2**, and **(P3)F2M** complexes are nearly 3 times higher than those of **DMA**, indicating that the **DMA** complexes have more MLCT character in the emitting state. The Stokes shifts and ($^1E_1$) − ($^3E_1$) values are demonstrated in Figure 6b. Thus, shorter lifetimes, higher k_r values, lower Stokes shifts, and lower ($^1E_1$) − ($^3E_1$) values of the **DMA** complexes attribute more MLCT character in their emitting states.

To further check the MLCT character in these complexes, we tried to correlate the radiative rate constants to the Einstein coefficient for spontaneous emission[48] by the equation

$$k_r = \frac{4E_{em}^{\ 3}}{3\bar{h}^4}|\langle\psi_e|\vec{d}|\psi_g\rangle|^2 \qquad (2)$$

where E_{em} is the emission energy in ergs, ψ_e and ψ_g are the wave functions for the excited and ground electronic states, and d is the transition dipole moment operator. Equation 2 implies that k_r/E_{em}^3 (with units of s/g) is proportional to the transition probability from the excited state to the ground state. The k_r/E_{em}^3 values of the complexes **(P1)DMA**, **(P3)DMA**, **(P350)DMA**, **(P3)F2**, **(P3)2F2**, and **(P3)F2M** are 0.081, 0.067, 0.068, 0.066, 0.053, and 0.096 erg s^{-1}, respectively. Thus, the transition probability of the **P3** complexes follows the order **(P3)F2M** > **(P3)DMA** > **(P3)F2**. Among the **DMA** complexes, the transition probability is maximum for **(P1)DMA**. Between the **(P3)F2** and **(P3)2F2** complexes, the former has more transition probability than the latter. Tentatively, we find that the methyl and dimethylamino groups increase the transition probability and the $-O-(CH_2CH_2O)_3-CH_3$ substituents in phosphine decrease the transition probability.

Furthermore, it has been shown[49] that the difference in ^{1}MLCT and ^{3}MLCT energies, ($^1E_1$) − ($^3E_1$), is related to the extinction coefficients and radiative rates of the polypyridyl complexes of Ru, Os, and Ir. For smaller ($^1E_1$) − ($^3E_1$) values, higher extinction coefficients of the absorption band, and higher k_r values, the MLCT character is larger. This also leads to higher transition probability. In the present study, the **DMA** complexes satisfy the above conditions and are presumed to have more MLCT character in the emitting state and higher transition probability. However, due to the depopulation of the excited

TABLE 4: Electroluminescence Properties

compound	λ_{em} (nm)	CIE (x, y)	max η_{ex} (%) (η_L) (cd/A)[a]	η_{ex} (%) η_L (cd/A)[a] at 1 mA/cm^2	η_{ex} (%) η_L (cd/A)[a] at 10 mA/cm^2	η_{ex} (%) η_L (cd/A)[a] at 100 mA/cm^2	turn-on V	max brightness (cd/m^2)
P(1)DMA	491	0.19, 0.34	1.61 (3.18)	1.61 (3.18)	1.41 (2.88)	0.7 (1.57)	7.6	1565
P(350)DMA	495	0.20, 0.37	1.62 (3.62)	1.51 (3.28)	1.34 (2.88)		8.2	1256
P(3)F2	486	0.19, 0.34	1.88 (3.8)	1.59 (3.28)	1.46 (3.02)	1.26 2.6	7.4	3814
P(3)2F2	486	0.18, 0.33	0.9 (1.8)	0.76 (1.44)	0.9 (1.8)	0.7 (1.40)	8.6	1641
P(3)F2M	491	0.19, 0.35	2 (4.13)	1.77 (3.62)	1.67 (3.5)	1.59 (3.3)	7.2	7200

[a] The luminance efficiencies are included in the parentheses.

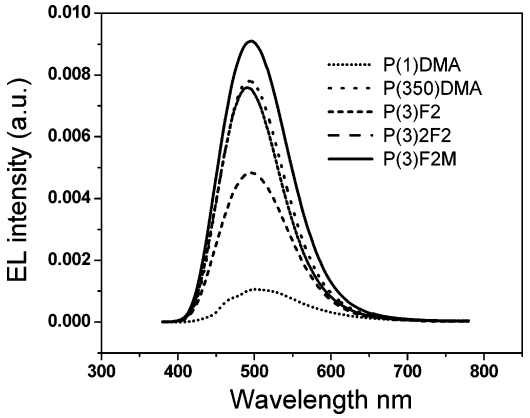

Figure 7. EL spectra obtained from the devices at 10 mA.

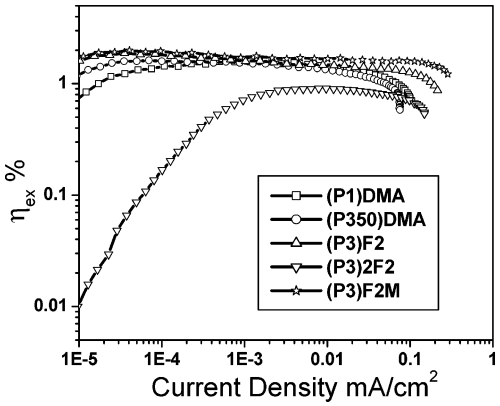

Figure 8. External quantum efficiencies of the EL devices plotted against current density.

state from the distortion of the dimethylamino group, the **DMA** complexes have more k_{nr} values and less quantum efficiency. This is also reflected in their transition probabilities in the sequence **(P3)F2M** > **(P3)DMA** > **(P3)F**2, as discussed above. The opposite effects of the $(^1E_1) - (^3E_1)$ and k_{nr} values leads to the lower transition probabilities of **(P3)DMA** compared to **(P3)F2M.** In the DMA ligand system, all three complexes have similar $(^1E_1) - (^3E_1)$ values. However, the k_r value of **(P1)DMA** is higher than those of **(P3)DMA** and **(P350)DMA** and hence the transition probability of **(P1)DMA** has a higher value than the other two **DMA** complexes. We presume that the longer glycolate groups could have some effect in decreasing the transition dipole moment.

Electroluminescence. Multilayer organic light emitting devices are fabricated by doping the complexes **(P1)DMA**, **(P350)DMA**, **P(3)F2**, **P(3)2F2**, and **P(3)F2M** (6 wt %) in a blend of polystyrene and *m*CP with the configuration of ITO/PEDOT−PSS (50 nm)/PS−*m*CP−dopant (20:74:6)/BAlq (40 nm)/LiF (0.9 nm)/Al (200 nm). Polystyrene is used as a binder in the present case, as neither *m*CP nor the complexes have good film forming properties if spun cast alone. There have been several reports of solid-state light emitting devices using polystyrene[50] and PMMA as binders. The electroluminescence (EL) characteristics are summarized in Table 4, and the EL spectra of the devices are shown in Figure 7. The EL spectra are red shifted and quite different in terms of the shape of the spectra compared with the PL spectra in the polystyrene matrix. The peak emissions are observed in the region 485−495 nm, where a shoulder is generally found in the PL spectrum of all of these complexes. The CIE coordinates are also shifted from the deep blue region to the sky blue region. We attribute such spectral changes to the effect of the matrix on the excited state of the complexes. The complexes contain three nonequivalent ligands including the polarizing cyano group, thus providing highly polar characteristics to the complexes. In such cases, the electronic charge distribution of the dopant in the excited state can be affected by the positive and negative polarons surrounding the dopant.[51] As PS[52] and *m*CP have different polar characteristics, the combinations of these materials under electrical excitation would generate different local electric fields inside the organic films and subsequently influence the excited state charge and nuclear distribution of the emitting dopant. We postulate that such phenomena alter the disposition of the energy levels and favor emission at lower energy.

The luminance efficiencies and the I−V−L characteristics of the complexes of the devices are shown in Figures 8 and 9, respectively. The **(P3)F2M** device demonstrates the best performance with a maximum external quantum efficiency (η_{ex}) of 2%, luminance efficiency (η_L) of 4.13 cd/A at 0.04 mA/cm^2, a maximum brightness of 7200 cd/m^2, and a 7.2 turn-on voltage. This is in agreement with the highest PL quantum efficiency of the **(P3)F2M** complex. The **(P3)F2** complex gives a maximum external quantum efficiency (η_{ex}) of 1.88%, η_L of 3.81 cd/A at 0.03 mA/cm^2, and a maximum brightness of 3814 cd/m^2 with a 7.4 turn-on voltage. A much lower η_{ex} value of 0.9% and η_L value of 1.8 cd/A were observed for the **P(3)2F2** device. Although **(P3)2F2** shows a higher PL efficiency (66%) than **(P3)F2**, specific reasons for the reduced EL device efficiency for **(P3)2F2** are not known yet. The incorporation of the $O-(CH_2CH_2O)_3-CH_3$ group in phosphine could control the aggregate formation of the dopants. However, when two phenyl groups are replaced by the $-O-(CH_2CH_2O)_3-CH_3$ groups in the **(P3)2F2** complex, charge conduction would be reduced as the nonconducting $-(CH_2CH_2O)-$ units could prevent the charge hopping, leading to a smaller number of excitons formed in the emitting layer. This is also manifested in the current−voltage and luminance characteristics, indicating that as the

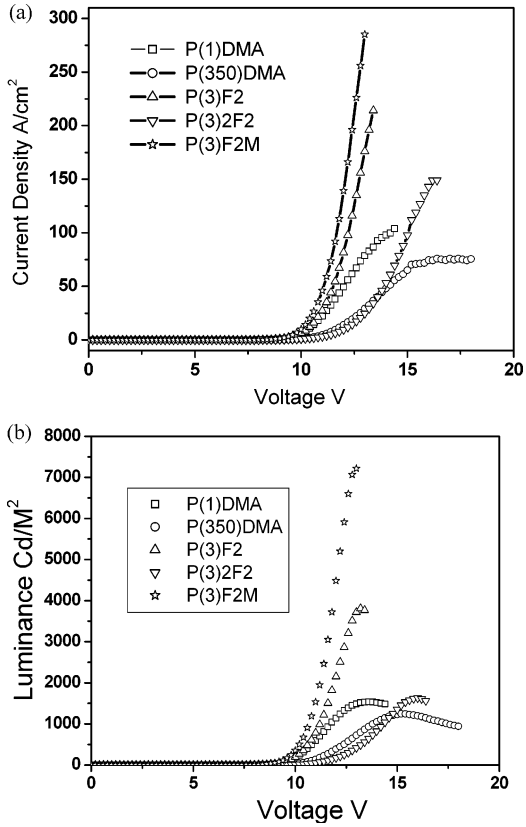

Figure 9. (a) Plot of current vs voltage and (b) brightness of the EL devices as a function of voltage.

number of $-O-(CH_2CH_2O)_3-CH_3$ substituents on the phosphine increases, the turn-on voltage increases and the brightness decreases. Thus, even if the complexes **(P3)F2** and **(P3)2F2** do not demonstrate any big difference in the PL properties, the EL efficiency of the **(P3)2F2** based device is almost half of the EL efficiency of the **(P3)F2** based device due to the reasons mentioned above.

Comparing **(P1)DMA** and **(P350)DMA**, it is noticed that both of them exhibit similar η_{ex} values of 1.61%. The latter exhibits a higher luminance efficiency of 3.5 cd/A at 0.07 mA/cm^2 and an 8.2 turn-on voltage, while **(P1)DMA** shows a maximum efficiency of 3.18 at 0.07 mA/cm^2 and a 7.6 turn-on voltage. Thus, the increase of ethylene glycol chain length results in higher luminance efficiency presumably due to the prevention of aggregates. On the other hand, the glycol chain length increases the turn-on voltage which results in almost similar external quantum efficiencies of both the **(P1)DMA** and **(P350)DMA** devices. It is interesting to note that while the PL efficiency of the DMA complexes is less than half of that of the **(P3)F2M** and **(P3)F2** complexes, the EL efficiency does not vary to that extent. We presume that, as the triplets of the dopant (2.85−2.8 eV) and the host *m*CP (2.9 eV) are quite close, there is a possibility of the exciton quenching on the dopant due to the backward energy transfer from the dopant[21] to the host *m*CP regardless of the difference in PL efficiency.

Conclusions

Bright deep blue emitting mixed ligand bis-cyclometalated Ir(III) complexes consisting of the cyclometalating, cyano, and phosphine ligands were synthesized. The influence of the number of $-(CH_2CH_2O)-$ units is pronounced in the thermal properties of the complexes. The average Ir−C(ring) bond distances are longer than the expected value and are ascribed to the *trans effect* of the strong phosphine and cyano ligands. The DFT calculations show that the d-orbitals of the iridium, π-orbitals of the cyclometalating ligand, and the cyano group contribute together to the HOMO, whereas the LUMO spreads over on one of the cyclometalating ligands. The HOMO and LUMO energy levels of the dimethylamino-substituted complexes are increased compared with the unsubstituted and methyl-substituted complexes. The transition probability from the excited state to the ground state of the **P3** complexes follows the order **(P3)F2M** > (**P3)DMA** > **(P3)F2**. Dimethylamino substitutution reduces the photoluminescence efficiency of the parent complex down to half, whereas the methyl substitution increases the quantum efficiency by 20%. This is attributed to the increase in the basicity of the dimethylamino group in the $DMAF_2ppy$ complexes upon excitation, leading to distortions and consequent nonradiative depopulation of the excited state. The effect of the substituents in phosphine is more pronounced in the EL than in the PL properties. Among the devices in the present study, the **(P3)F2M** based device shows the best performance with an η_{ex} value of 2% and an η_L value of 4.13 cd/A at 0.04 mA/cm^2, a maximum brightness of 7200 cd/m^2 and a lowest turn-on voltage of 7.2 V followed by the **(P3)F2** based device. On the other hand, the dimethylamino substitution decreases the device efficiency. **(P1)DMA** and **(P350) DMA** based devices indicate that a greater number of $-(CH_2CH_2O)-$ units in the phosphine ligand increases the device efficiency, as it could decrease the quenching of excitons or trapped charges by preventing aggregation in the emitting layer. As observed, one or two $-O-(CH_2CH_2O)_3-CH_3$ substituents in the phosphines **(P3)** and **(P3)2** do not demonstrate any big difference in the PL properties of the corresponding complexes **(P3)F2** and **(P3)2F2**, respectively, but the EL efficiency of the **(P3)2F2** based device is almost half of the EL efficiency of the **(P3)F2** based device probably due to lesser charge conduction and subsequent decrease in the exciton formation in the device. A shift of the Commission Internationale de L'Eclairage (CIE) coordinate from deep blue (0.15, 0.09)−(0.14, 0.16) in PL to sky blue (0.19, 0.35) in EL is observed in all of the complexes. We presume that the use of a suitable host with a higher triplet energy would increase the device efficiency and improve the color purity.

Acknowledgment. The authors are thankful to Professor Myoung Soo Lah at Hanyang University for providing the data of single crystal X-ray diffraction and Professor Chongmok Lee at Ewha Women's University for the cyclovoltametric studies. K.C. thanks the NANO System Institute-National Core Research Center (NCRC) from the Korea Science and Engineering Foundation (KOSEF) for the financial support.

Supporting Information Available: Crystallographic information for **(P1)DMA** and **(P3)F2M** (CIF files), synthesis of the phosphine ligands **P1**, **P3**, and **P350**, the reaction scheme of the complexes, the experimental methods for the spectroscopic measurements, cyclic voltammetry, and OLED fabrication and characterization. This material is available free of charge via the Internet at http://pubs.acs.org.

References and Notes

(1) (a) King, K. A.; Spellane, P. J.; Watts, R. J. *J. Am. Chem. Soc.* **1985**, *107*, 1431. (b) Dedeian, K.; Djurovitch, P. I.; Garces, F. O.; Carlson, G.; Watts, R. J. *Inorg. Chem.* **1991**, *30*, 1685. (c) Garces, F. O.; King, K. A.; Watts, R. J.; *Inorg. Chem.* **1988**, *27*, 3464.

(2) (a) Baldo, M. A.; Lamansky, S.; Burrows, P. E.; Thompson, M. E.; Forrest, S. R. *Appl. Phys. Lett.* **1999**, *75*, 4. (b) Adachi, C.; Baldo, M. A.; Forrest, S. R.; Thompson, M. E.; *Appl. Phys. Lett.* **2000**, *77*, 904. (c) Kawamura, Y.; Yanagida, S.; Forrest, S. R. *J. Appl. Phys.* **2002**, *92*, 87. (d) T. Tsutsui, T.; Yang. M. J.; Yahoro, M.; Nakamura, K.; Watanabe, T.;

Suji, T.; Fukuda, Y.; Wakimoto, T.; Miyaguchi, S. *Jpn. J. Appl. Phys., Part 2* **1999**, *38*, L1502.

(3) (a) Maestri, M.; Balzani, V.; Deuschel-Cornioley, C.; von Zelewsky, A.; *Adv. Photochem.* **1992**, *17*, 1. (b) Colombo, M. G.; Brunold, T. C.; Riedener, T.; Gudel, H. U.; Fortsch, M.; Burgi, H.-B. *Inorg. Chem.* **1994**, *33*, 545−550. (c) Ohsawa, Y.; Sprouse, S.; King, K. A.; DeArmond, M. K.; Hanck, K. W.; Watts, R. J. *J. Phys. Chem.* **1987**, *91*, 1047. (d) Colombo, M. G.; Gudel, H. U. *Inorg. Chem.* **1993**, *32*, 3088. (e) Maestri, M.; Sandrini, D.; Balzani, V.; Maeder, U.; von Zelewsky, A. *Inorg. Chem.* **1987**, *26*, 1323. (f) Lever, A. B. P. *Inorganic Electronic Spectroscopy*, 2nd ed.; Elsevier: New York, 1984; pp 174−178.

(4) (a) Förster, T. *Discuss. Faraday Soc.* **1959**, *27*, 7. (b) Dexter, D. L. *J. Chem. Phys.* **1953**, *21*, 836. (c) Baldo, M. A.; Thompson, M. E.; Forrest, S. R. *Nature* **2000**, *403*, 750.

(5) (a) Adachi, C.; Baldo, M. A.; Thompson, M. E.; Forrest, S. R. *J. Appl. Phys.* **2001**, *90*, 5048. (b) Xie, H. Z.; Liu, M. W.; Wang, O. Y.; Zhang, X. H.; Lee, C. S.; Hung, L. S.; Lee, S. T.; Teng, P. F.; Kwong, H. L.; Zheng, H.; Che, C. M. *Adv. Mater.* **2001**, *13*, 1245. (c) Wang, Y.; Herron, N.; Grushin, V. V.; LeCloux, D.; Petrov, V. *Appl. Phys. Lett.* **2001**, *79*, 449.

(6) (a) Yeh, S.-J.; Wu, M.-F.; Chen, C.-T.; Song, Y.-H.; Chi, Y.; Ho, M.-H.; Hsu, S.-F.; Chen, C. H. *Adv. Mater.* **2005**, *17*, 285. (b) Li, C.-L.; Su, Y.-J.; Tao, Y.-T.; Chou, P.-T.; Chien, C.-H.; Cheng, C.-C.; Liu, S.-R. *Adv. Funct. Mater.* **2005**, *15*, 387. (c) Chen, X.; Liao, J.-L.; Liang, Y.; Ahmed, M. O.; Tseng, H.-E.; Chen, S. A. *J. Am. Chem. Soc.* **2003**, *125*, 636

(7) (a) Tanaka, I.; Tabata, Y.; Tokito, S. *Chem. Phys. Lett.* **2004**, *400*, 86. (b) Coppo, P.; Plummer, E. A.; De Cola, L. *Chem. Commun.* **2004**, 1774. (c) Holmes, R. J.; Forrest, S. R.; Tung, Y.-J.; Kwong, R. C.; Brown, J. J.; Garon, S.; Thompson, M. E. *Appl. Phys. Lett.* **2003**, *82*, 2422. (d) Ren, X.; Li, J.; Holmes, R. J.; Djurovich, P. I.; Forrest, S. R.; Thompson, M. E. *Chem. Mater.* **2004**, *16*, 4743.

(8) (a) Lamansky, S.; Djurovich, P.; Murphy, D.; Abdel-Razzaq, F.; Lee, Hae-Eun.; Adachi, C.; Burrows, P. E.; Forrest, S. R.; Thompson, M. E. *J. Am. Chem. Soc.* **2001**, *123*, 4304−4312. (b) Brooks, J.; Babayan, Y.; Lamansky, S.; Djurovich, P. I.; Tsyba, I.; Bau, R.; Thompson, M. E. *Inorg. Chem.* **2002**, *41*, 3055−3066. (c) Tokito, S.; Suzuki, M.; Sato, F.; Kamachi, M.; Shirane, K. *Org. Electron.* **2003**, *4*, 105.

(9) (a) Li, J.; Djurovitch, P. I.; Alleyene, B. D.; Yousufudin, M.; Ho, N. N.; Thomas, J. C.; Peters, J. C.; Bau, R.; Thompson, M. E. *Inorg. Chem.* **2005**, *44*, 1713−1727. (b) Yeh, S.-J.; Wu, M.-F.; Chen, C.-T.; Song, Y.-H.; Chi, Y.; Ho, M.-H.; Hsu, S.-F.; Chen, C. H. *Adv. Mater.* **2005**, *17*, 285−289. (c) Dedeian, K.; Shi, J.; Shepherd, N.; Forsythe, E.; Morton, D. C. *Inorg. Chem.* **2005**, *44*, 4445.

(10) (a) Tokito, S.; Lijima, T.; Suzuri, Y.; Kita, H.; Suzuki, M.; Sato, F. *Appl. Phys. Lett.* **2003**, *83*, 569−571. (b) Tokito, S.; Suzuki, M.; Sato, F.; Kamachi, M.; Shrane, K. *Org. Electron.* **2003**, *4*, 105.

(11) Jian, L.; Djurovich, P. I.; Alleyne, B. D.; Yousufuddin, M.; Ho, N. N.; Thomas, J. C.; Peters, J. C.; Bau, R.; Thompson, M. E. *Inorg. Chem.* **2005**, *44*, 1713.

(12) Lee, C.-L.; Das R. R.; Kim, J.-J. *Chem. Mater.* **2004**, *16*, 4642.

(13) Yu, J.-K.; Hu, Y.-H.; Cheng, Y.-M.; Chou, P.-T.; Peng, S.-M.; Lee, G.-H.; Carty, A. J.; Tung, Y.-L.; Lee, S.-H.; Chi, Y.; Liu, C.-S. *Chem.−Eur. J.* **2004**, *10*, 6255−6264.

(14) Tamayo, A. B.; Alleyene, B. D.; Djurovitch, P. I.; Lamansky, S.; Tsyba, Y.; Ho, N. N.; Bau, R.; Thompson, M. E. *J. Am. Chem. Soc.* **2003**, *125*, 7377−7387.

(15) Adamovich, V. I.; Cordero, S. R.; Djurovich, P. I.; Tamayo, A. B.; Thompson, M. E.; D'Andrade, B. W.; Forrest, S. R. *Org. Electron.* **2003**, *4*, 77−87.

(16) (a) Nakamura, A.; Tada, T.; Mizukami, M.; Yagyu, S. *Appl. Phys. Lett.* **2004**, *84*, 130. (b) Yang, X.; Neher, D.; Hertel, D.; Daubler, T. K. *Adv. Mater.* **2004**, *161*, 4070.

(17) Zhu, W.; Liu, C.; Su, L.; Yang, W.; Yuan, M.; Cao, Y. *J. Mater. Chem.* **2003**, *13*, 50.

(18) (a) Lee, C.-L.; Lee, K.-B.; Kim, J.-J. *Appl. Phys. Lett.* **2000**, *77*, 2280. (b) Yang, M. J.; Tsutsui, T. *Jpn. J. Appl. Phys.* **2000**, *39*, L828. (c) Gong, X.; Robinson, M. R.; Ostrowski, J. C.; Moses, D.; Bazan, G. C.; Heeger, A. J. *Adv. Mater.* **2002**, *14*, 581. (d) Markham, J. P. J.; Anthopoulos, T.; Magennis, S. W.; Burn, P. L.; Samuel, I. D. W. *Appl. Phys. Lett.* **2002**, *80*, 2645.

(19) Adamovich, V.; Brooks, J.; Tamayo, A.; Alexander, A. M.; Djurovich, P. I.; D'Andrade, B. W.; Adachi, C.; Forrest, S. R.; Thompson, M. E. *New J. Chem.* **2002**, *26*, 1171.

(20) Noh, Y.-Y.; Lee, C.-L.; Kim, J.-J. *J. Chem. Phys.* **2003**, *118*, 2853−2864.

(21) Adachi, C.; Kwong, R. C.; Djurovich, P. I.; Adamovich, V.; Baldo, M. A.; Thompson, M. E.; Forrest, S. R. *Appl. Phys. Lett.* **2001**, *79*, 2082−2084.

(22) Sprouse, S.; King, K. A.; Spellane, P. J.; Watts, R. J. *J. Am. Chem. Soc.* **1984**, *106*, 6647.

(23) Bard, A. J.; Faulkner, L. R. *Electrochemical Methods: Fundamentals and Applications*, 2nd ed.; Wiley: New York, 2001; p 811.

(24) Sheldrick, G. M. *SHELXTL-PLUS, Crystal Structure Analysis Package*; Bruker Analytical X-ray: Madison, WI, 1997.

(25) Garces, F. O.; Dedian, K.; Keder, N. L.; Watts, R. J. *Acta Crystallogr.* **1993**, *C49*, 1117.

(26) Urban, R.; Kramer, R.; Mihan, S.; Polborn, K.; Wagner, B.; Beck, W. J. *Organomet. Chem.* **1996**, *517*, 191.

(27) Neve, F.; Crispini, A. *Eur. J. Inorg. Chem.* **2000**, 1039.

(28) Tolman, C. A. *Chem. Rev.* **1977**, *77*, 313.

(29) Koch, W.; Holthausen, M. C. *A Chemist's Guide to Density Functional Theory*; Wiley & Sons: New York, 2000.

(30) Parr, R. G.; Yang, W. *Density Functional Theory of Atoms and Molecules*; Oxford University Press: Oxford, U.K., 1989.

(31) Becke, A. D. *J. Chem. Phys.* **1993**, *98*, 5648−5652.

(32) Hay, P. J.; Wadt, W. R. *J. Chem. Phys.* **1985**, *82*, 299.

(33) (a) Gross, E. K. U.; Kohn, W. *Adv. Quantum Chem.* **1990**, *21*, 255. (b) Bauernschmitt, R.; Ahlrichs, R. *Chem. Phys. Lett.* **1998**, *256*, 454.

(34) (a) Casida, M. E.; Jamorski, C.; Casida, K. C.; Salahub, D. R. *J. Chem. Phys.* **1998**, *108*, 4439. (b) Wiberg, K. B.; Stratmann, R. E.; Frisch, M. J. *Chem. Phys. Lett.* **1998**, *297*, 60.

(35) Frisch, M. J.; Trucks, G. W.; Schlegel, H. B.; Scuseria, G. E.; Robb, M. A.; Cheeseman, J. R.; Zakrzewski, V. G.; Montgomery, J. A., Jr.; Stratmann, R. E.; Burant, J. C.; Dapprich, S.; Millam, J. M.; Daniels, A. D.; Kudin, K. N.; Strain, M. C.; Farkas, O.; Tomasi, J.; Barone, V.; Cossi, M.; Cammi, R.; Mennucci, B.; Pomelli, C.; Adamo, C.; Clifford, S.; Ochterski, J.; Petersson, G. A.; Ayala, P. Y.; Cui, Q.; Morokuma, K.; Malick, D. K.; Rabuck, A. D.; Raghavachari, K.; Foresman, J. B.; Cioslowski, J.; Ortiz, J. V.; Stefanov, B. B.; Liu, G.; Liashenko, A.; Piskorz, P.; Komaromi, I.; Gomperts, R.; Martin, R. L.; Fox, D. J.; Keith, T.; Al-Laham, M. A.; Peng, C. Y.; Nanayakkara, A.; Gonzalez, C.; Challacombe, M.; Gill, P. M. W.; Johnson, B. G.; Chen, W.; Wong, M. W.; Andres, J. L.; Head-Gordon, M.; Replogle, E. S.; Pople, J. A. *Gaussian 98*, revision A.9; Gaussian, Inc.: Pittsburgh, PA, 1998.

(36) Li, J.; Djurovich, P. I.; Alleyene, B. D.; Yousuffudin, M.; Ho, N. N.; Thomas, J. C.; Peters, J. C.; Bau, R.; Thompson, M. E. *Inorg. Chem.* **2005**, *44*, 1713.

(37) (a) Park, N. G.; Choi, G. C.; Lee, J. E.; Kim Y. S. *Curr. Appl. Phys.* **2005**, *5*, 79. (b) Kwon, T.-H.; Cho, H. S.; Kim, M. K.; Kim, J.-W.; Kim, J.-J.; Lee, k. H.; Park, S. J.; Shin, I.-S.; Kim, H.; Shin, D. M.; Chung, Y. K.; Hong, J.-I. *Organometallics* **2005**, *24*, 1578. (c) Polson, M.; Ravaglia, M.; Fracasso, S.; Garavelli, M.; Scandola, F. *Inorg. Chem.* **2005**, *44*, 1282.

(38) Kulikova, M. V.; Balashev, K. P.; Kvam, P. I.; Songstad, J. *Russ. J. Gen. Chem.* **1999**, *69*, 1521.

(39) (a) Nicholson, R. S.; Shain, I. *Anal. Chem.* **1964**, *36*, 706. (b) Kim. J. Y.; Lee, C.; Park, J. W. J. *J. Electroanal. Chem.* **2001**, *504*, 104.

(40) Turner, J. A.; Christi, J. H.; Vukovic, M.; Osteryong, R. A. *Anal. Chem.* **1977**, *49*, 843.

(41) Hwang, F.-M.; Chen, H.-Y.; Chen, P.-S.; Liu, C.-S.; Chi, Y.; Shu, C. F.; Wu, F.-L.; Chou, P.-T.; Peng, S.-M.; Lee, G.-H. *Inorg. Chem.* **2005**, *44*, 1344.

(42) (a) Garces, F. O.; King, K. A.; Watts, R. J. *Inorg. Chem.* **1988**, *27*, 3464. (b) Carlson, G. A.; Pjurovich, P. I.; Watts, R. J. *Inorg. Chem.* **1993**, *32*, 4483. (c) Colombo, M. G.; Brunold, T. C.; Riedener, T.; Gudel, H. U.; Fortsch, M.; Burgi, H.-B. *Inorg. Chem.* **1994**, *33*, 545.

(43) Choi, C. L.; Phillips, D. L. *Mol. Phys.* **1998**, *94*, 547−554.

(44) (a) Tang, K.-C.; Liu, K. L.; Chen, I.-C. *Chem. Phys. Lett.* **2004**, *386*, 437. (b) Damrauer, N. H.; Cerullo, G.; Yeh, A.; Boussie, T. R.; Shank, C. V.; McCusker, J. K. *Science* **1997**, *275*, 54. (c) Damrauer, N. H.; McCusker, J. K. *J. Phys. Chem. A* **1999**, *103*, 8440. (d) Yeh, A. T.; Shank, C. V.; McCusker, J. K. *Science* **2000**, *289*, 935.

(45) Goushi, K.; Kwong, R.; Brown, J. J.; Sasabe, H.; Adachi, C. *Appl. Phys. Lett.* **2004**, *95*, 7798.

(46) (a) Caspar, J. V.; Meyer, T. J. *Inorg. Chem.* **1983**, *22*, 2444. (b) Rillema, D. P.; Blanton, C. B.; Shaver, R. J.; Jackman, D. C.; Boldaji, M.; Bundy, S.; Worl, L. A.; Meyer, T. J. *Inorg. Chem.* **1992**, *31*, 1600. (c) Kober, E. M.; Casper, J. V.; Lumpkin, R. S.; Meyer, T. *J. Phys. Chem.* **1986**, *90*, 3722.

(47) Dobokowski, J.; Michl, J.; Waluk, J. *Phys. Chem. Chem. Phys.* **2003**, *5*, 1027.

(48) (a) Allen, G. H.; White, R. P.; Rillema, D. P.; Meyer, T. J. *J. Am. Chem. Soc.* **1984**, *106*, 2613. (b) Herzberg, G. *Molecular Spectra and Molecular Structure*; Van Nostrand: New York, 1950; Vol. 1.

(49) (a) Demas, J. N.; Crosby, G. A. *J. Am. Chem. Soc.* **1971**, *93*, 2841. (b) Watts, R. J.; Crosby, G. A.; Sansregret, J. L. *Inorg. Chem.* **1972**, *11*, 1474.

(50) (a) Rudmann, H.; Rubner M. F. *J. Appl. Phys.* **2001**, *90*, 4338. (b) Rudmann, H.; Shimada, S.; Rubner M. F. *J. Am. Chem. Soc.* **2002**, *124*, 4918.

(51) Rabeck, J. F. *Mechanisms of Photophysical Processes and Photochemical Reactions in Polymers: Theory and Applications*; Wiley: Chichester, U.K., 1987.

(52) Park, J. H.; Park, O. O.; Yu, J.-W.; Kim, J. K.; Kim, Y. C. *Appl. Phys. Lett.* **2004**, *84*, 1783.